Proceedings of the Project Review, Geo-Mathematical Imaging Group (Purdue University, West Lafayette IN), Vol. 1 (2013) pp. 291-302.

INTERFACE WAVES ALONG FRACTURES IN TRANSVERSELY ISOTROPIC MEDIA

SIYI SHAO* AND LAURA J. PYRAK-NOLTE†

Abstract. An analytical solution for fracture interface waves that propagated along fractures in a transversely isotropic medium was derived for fractures oriented parallel and perpendicular to the layering. From the theoretical derivation, the existence of fracture interface waves can mask the textural shear wave anisotropy of waves propagated parallel to the matrix layering. In a case of an intact layered garolite sample, the ratio of v_{SH} (velocity of a shear wave polarized parallel to the background layering) to v_{SV} (velocity of a shear wave polarized perpendicular to the layering) was approximately 1.06. However, in the fractured samples, the observed shear wave velocity ratio (v_{SH} divided by v_{SV}) was dependent upon the stress and orientation of the fracture relative to the layering. When the fracture was oriented perpendicularly to the layering, the shear wave velocity ratio was around 1.02 at lower stress because of the existence of fracture interface waves that propagate with speeds slower than the bulk SH wave velocity. The ratio increased to the intact value with increasing stress. When the fracture was oriented parallel to the layering, the shear wave velocity ratio was around 1.12 at low stress and decreased to 1.06 as the stiffness of fracture increased with increasing stress. Shear fracture specific stiffness was estimated for the fractured samples using the derived analytical solution. The interface wave theory demonstrates that the interpretation of the presence of fractures in anisotropic material can be unambiguously interpreted if experimental measurements are made as a function of stress which eliminates many fractured-generated discrete modes such as fracture interface waves.

1. Introduction. Discontinuities such as fractures, joints and faults occur in the Earth's crusts in a variety of rock types. While much theoretical, experimental and computational research has examined seismic wave propagation in fractured isotropic rocks, fewer studies have examined seismic wave propagation in fractured anisotropic rocks (e.g., Carcione, 1996; Kundu, 1996; Carcione, 1998; Rüger, 1998; Chaisri, 2000; Carcione, 2012). Because the detection of fractures in an anisotropic medium is complicated by discrete modes that are guided or confined by fractures, i.e., Fracture interface wave, as well as the anisotropic matrix, to understand the interaction between those two mechanism of anisotropy (fractures and matrix) becomes the major objective of this paper.

Previous research has shown theoretically and experimentally that the existence of coupled Rayleigh waves or fracture interface waves, along fractures in isotropic material (e.g., Murty, 1975; Pyrak-Nolte, 1987; Suarez-Rivera, 1992; Gu, 1996). The existence of those waves depends on the wavelength of the signal and the fracture specific stiffness relative to the material properties of the matrix. Nihei et al. (1999) showed theoretically the existence of Love waves in an isotropic medium, where the Love waves are guided by the presence of parallel fractures (Nihe et al., 1999) . Xian et al. (2001) demonstrated experimentally that leaky-compressional wave guided modes, that can travel over 60 wavelengths, occur in sets of parallel fractures in an isotropic medium and are sensitive to the stiffness distributions within the fracture sets (Xian et al. 2001).

Over the last decade, several researchers have made theoretical progress in studying fractures in anisotropic media. For example, Schoenberg derived a second rank compliance tensor (inverse of stiffness tensor) for a vertically fractured transversely isotropic medium with a set of parallel fractures to theoretically deconstruct the contribution from the fractures versus that from the matrix (see Schoenberg, 2009). Diner applied the method by Schoenberg and obtained the fracture and background medium parameters for a monoclinic compliance tensor (Diner, 2011). However, these effective medium approaches ignore the existence of fracture interface waves and other fracture guided modes that can affect seismic interpretation. Because these guided modes are frequency dependent, broadband data can result in the observation of both effective medium as well as discrete mode behavior, i.e. overlapping scattering regimes. For example, Nolte et al. (2000) demonstrated experimentally that different scattering regimes coexist when broadband sources are used (Nolte et al. 2000). Specifically, they observed the transition from long wavelength to short wavelength scattering behavior for fracture interface waves was a smooth transition where both interface waves

*Physics Department, Purdue University, West Lafayette, IN (shao5@purdue.edu)

†Physics Department, School of Civil Engineering, and the Department of Earth and Atmospheric Sciences, Purdue University, West Lafayette, IN

and resonant-scattered Rayleigh waves were observed.

In this study, we demonstrate, theoretically, that fracture interface waves can complicate the interpretation of seismic anisotropy of a transversely isotroic medium for shear waves propagated through the layering. The next section briefly introduced the interface wave theory for two different fracture orientations relative to the layered matrix. In the following section, we discussed the apparent shear wave anisotropy of two fracture orientations. We found the orientation of the fracture relative to the layering can make materials appear isotropic or of stronger anisotropy than the matrix anisotropy, because of the existence of fracture interface waves; and the background or matrix anisotropy is recovered through the application of stress normal to the fracture plane that closes the fracture.

2. Theory. Theoretical derivations for dispersive fracture interface waves in fractured isotropic material can be traced back to previous work (e.g., Pyrak-Nolte et al., 1987 and Gu et al., 1996). A thin fracture can be described using a boundary condition (often referred as displacement discontinuity theory or linear-slip theory) as: stress across a fracture is continuous, but the displacement is not. The discontinuity in displacement is inversely proportional to the specific stiffness of the fracture (Mindlin, 1960; Kendall, 1971; Murty, 1975; Schoenberg, 1980; Kitsunezaki, 1983; Schoenberg, 1983; Myer, 1985; Pyrak-Nolte, 1988; Pyrak-Nolte, 1990a&b; Murty, 1991; Suarez-Rivera, 1992; Gu, 1994). Here we present theoretical derivations for fracture interface waves for a transversely isotropic (TI) medium with a single fracture oriented either parallel (we call it the FH medium), or perpendicular (the FV medium) to the layering of the matrix (Figure 1 and 3). The fracture for either medium is presented by non-welded contact between two identical material with same seismic properties: material density and elastic constants (wave velocities).

2.1. Fracture perpendicular to layering (FV). In the FV medium, a fracture is assumed to lie in the x-y plane (solid line in Figure 1). The first half space for z>0 is medium 1, and the sscond half space for z<0 is medium 2. The displacement discontinuity boundary conditions that

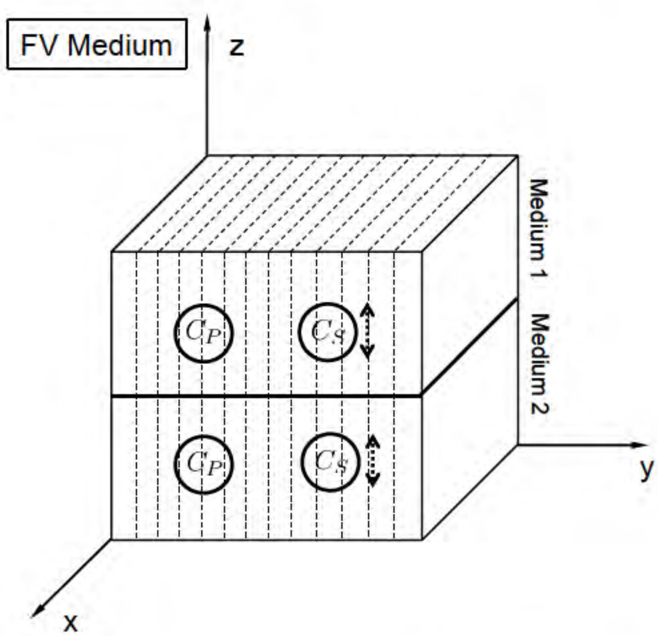

FIG. 1. *A sketch of the FV medium with a fracture lying in the x-y plane (solid line), while the layers lie in the x-z plane (dashed lines). C_P represents a compressional wave (P wave) propagating parallel to the layers in the x-y plane in media 1 and 2. C_S represents a shear wave (S wave) propagating parallel to the layers in the x-y plane, and are polarized parallel to layers as indicated by the dashed arrows in medium 1 and medium 2.*

represent the fracture are:

$$\begin{aligned} u_z^{(1)} - u_z^{(2)} &= \sigma_{zz}^{(1)}/\kappa_z, \\ \sigma_{zz}^{(1)} &= \sigma_{zz}^{(2)}, \\ u_x^{(1)} - u_x^{(2)} &= \sigma_{zx}^{(1)}/\kappa_x, \\ \sigma_{zx}^{(1)} &= \sigma_{zx}^{(2)}, \\ u_y^{(1)} - u_y^{(2)} &= \sigma_{zy}^{(1)}/\kappa_y, \\ \sigma_{zy}^{(1)} &= \sigma_{zy}^{(2)}, \end{aligned} \tag{2.1}$$

where κ_x and κ_y represent the shear specific stiffness of the fracture, κ_z is the normal specific stiffness, while σ is a second rank tensor representing stress across the fracture. Superscripts (1) and (2) indicate the parameters referred in medium 1 and medium 2.

The equations for the velocity of interface waves in an TI medium are expressed as following (see Appendix A for detailed derivation):

$$(1-2\xi^2)^2 - 4\xi^2\sqrt{\xi^2-\eta^2}\sqrt{\xi^2-1} - 2\overline{\kappa_z}\sqrt{\xi^2-\eta^2} = 0 \tag{2.2}$$

for the symmetric interface wave, and

$$(1-2\xi^2)^2 - 4\xi^2\sqrt{\xi^2-\eta^2}\sqrt{\xi^2-1} - 2\overline{\kappa_x}\sqrt{\xi^2-1} = 0 \tag{2.3}$$

for the antisymmetric interface wave, where $\xi = C_S/C, \eta = C_S/C_P$, ($C$ is the interface wave velocity, C_S and C_P are shear and compressional wave velocities as in Figure 1), $\overline{\kappa_z} = \kappa_z/\omega Z_S$ is the normalized normal stiffness, and $\overline{\kappa_x} = \kappa_x/\omega Z_S$ is the normalized shear stiffness ($Z_S = \rho C_S$ is the shear wave impedance, ρ is material density).

Table 2.1 lists all of the parameters from a fractured garolite sample (see Shao et al., 2012) to solve equation (2.2) and (2.3). Figure 2 shows the interface wave velocities (phase and group) normalized by the bulk shear wave velocity (polarized parallel to layers) as a function of normalized fracture stiffness $\overline{\kappa_z}(\overline{\kappa_x})$. Like the isotropic case, symmetric (fast) and antisymmetric (slow) modes exist with phase and group velocities that range from the Rayleigh velocity at low fracture specific stiffness (or high frequency), to bulk shear wave velocity at higher fracture specific stiffness (or low frequency).

Table 2.1
Parameter values in solving equations (2.2) and (2.3)

Parameters in Medium 1 and 2	Value
f (Frequency: MHz)	0.21
C_P (P wave velocity: m/s)	3060
C_S (S wave velocity: m/s)	1514
ρ (Density: kg/m^3)	1365

2.2. Fracture parallel to layering (FH). Similar to the FV medium, equations for symmetric and antisymmetric interface waves were also derived for the case when the fracture and the layers are parallel to each other (the FH medium, see Figure 3).

The equation for symmetric interface waves in the FH medium (see Appendix B for detailed derivation) can be expressed as:

$$\left(\frac{\eta_3}{\eta_1}\right)^2 \left[(2\xi^2-1)\left(2\xi^2 - \left(\frac{\eta_1\eta_2}{\eta_3}\right)^2\right) - 4\xi^2\sqrt{\xi^2-1}\sqrt{\xi^2-\eta_1^2}\right] - 2\sqrt{\xi^2-\eta_1^2}\cdot\overline{\kappa_z} = 0, \tag{2.4}$$

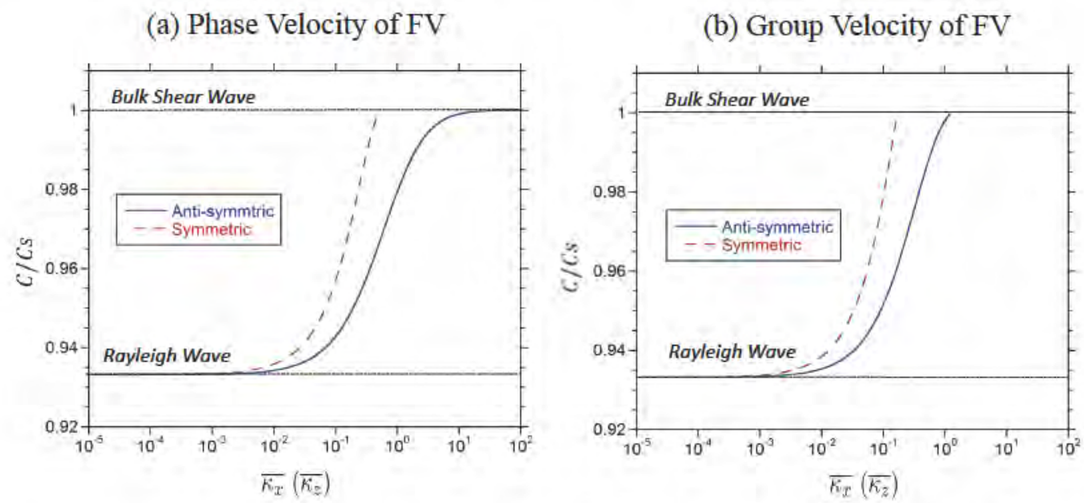

FIG. 2. *(a) Normalized interface wave phase velocity (C/C_S) as a function of normalized stiffness $\overline{\kappa_z} = \kappa_z/\omega Z_S$ for the FV medium; (b) Normalized interface wave group velocity as a function of normalized stiffness $\overline{\kappa_z}$.*

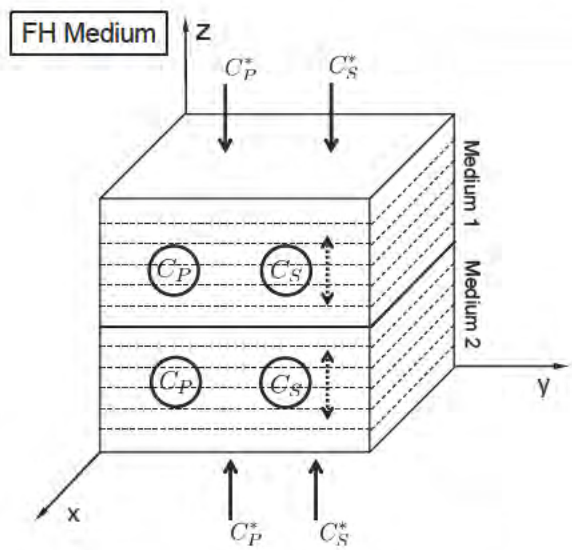

FIG. 3. *A sketch of the FH medium with both the fracture (solid line) and the layering (dashed line) lying in the x-y plane. C_P represents a compressional wave (P wave) propagating parallel to the layers in the x-y plane in media 1 and 2. C_S represents a shear wave (S wave) propagating parallel to the layers in the x-y plane, and are polarized parallel to layers as indicated by the dashed arrows in medium 1 and medium 2. C_P^* and C_S^* represent compressional (P) and shear (S) waves propagating along the z direction perpendicularly through the layers.*

and for the antisymmetric interface wave as:

$$\left(\frac{\eta_3\eta_4}{\eta_1^2\eta_2}\right)^2 \left[\left(2\xi^2 - 1\right)\left(2\xi^2 - \left(\frac{\eta_1\eta_2}{\eta_3}\right)^2\right) - 4\xi^2\sqrt{\xi^2 - 1}\sqrt{\xi^2 - \eta_1^2}\right] - 2\sqrt{\xi^2 - 1}\cdot\overline{\kappa_x} = 0, \tag{2.5}$$

where

$$\xi = C_S/C,$$
$$\eta_1 = C_S/C_P,$$
$$\eta_2 = C_P^*/C_P, \tag{2.6}$$
$$\eta_3 = C_S'/C_P,$$
$$\eta_4 = C_S^*/C_P.$$

In equation (2.6), C_S, C_P, C_S^* and C_P^* are S and P wave velocities, respectively, that can be found in Figure 3. C_S' is a notation that can be expressed in terms of the elastic components C_{33} and C_{13} (see Appendix B), and the material density ρ as:

$$C_S' = \sqrt{(C_{33} - C_{13})/2\rho}, \tag{2.7}$$

C_S, C_P, C_S^* and C_P^* were obtained from experimental measurements of S-waves and P-waves propagated either parallel or perpendicular to the layers (Figure 3), while C_S' can be obtained by fitting the Rayleigh wave velocity: comparing the "simulated" Rayleigh wave velocities with the experimentally measured Rayleigh wave velocity, or measuring azimuzally varied P-wave velocities in the FH medium.

Table 2.2 lists all of the parameters from a fractured garolite sample (Shao et al., 2012) to solve equation (2.4) and (2.5). Solutions corresponding to the symmetric and antisymmetric waves were found for the FH medium (the layering and the fracture are parallel). Figure 4 displays the normalized phase (Figure 4a) and group (Figure 4b) velocities as a function of normalized stiffness. Both the phase and group velocities exhibited similar trends as for the FV medium (Figure 2): symmetric and antisymmetric interface waves exist with phase and group velocities that range from Rayleigh velocity at low stiffness, to bulk shear wave velocities at higher stiffness.

Table 2.2
Parameter values in solving equations (2.4) and (2.5)

Parameters in Medium 1 and 2	Value
f (Frequency: MHz)	0.21
C_P (Horizonal P wave velocity: m/s)	2990
C_S (Horizontal S wave velocity: m/s)	1418
C_P^* (Vertical P wave velocity: m/s)	2271
C_S^* (Vertical S wave velocity: m/s)	1402
C_S' (m/s)	1094
ρ (Density: kg/m^3)	1365

3. Discussion. The existence of fracture interface waves can affect the interpretation of shear wave anisotropy of a transversely isotropic medium. Using the theoretically derived interface wave velocities for the FV and FH media, we examined the "apparent" shear wave anisotropy, and compared theoretical results with experimental results (Shao et al., 2012).

3.1. Shear wave anisotropy. To evaluate shear wave anisotropy, Thomsen (1986) introduced the following equation in terms of elastic components as (see Thomsen, 1986):

$$\gamma = \frac{C_{66} - C_{44}}{2C_{44}}, \tag{3.1}$$

where C_{66} can be expressed by shear waves polarized parallel to layers and propagating parallel to layers (which we refer to as a SH wave with a velocity of v_{SH}), and C_{44} can be expressed by shear

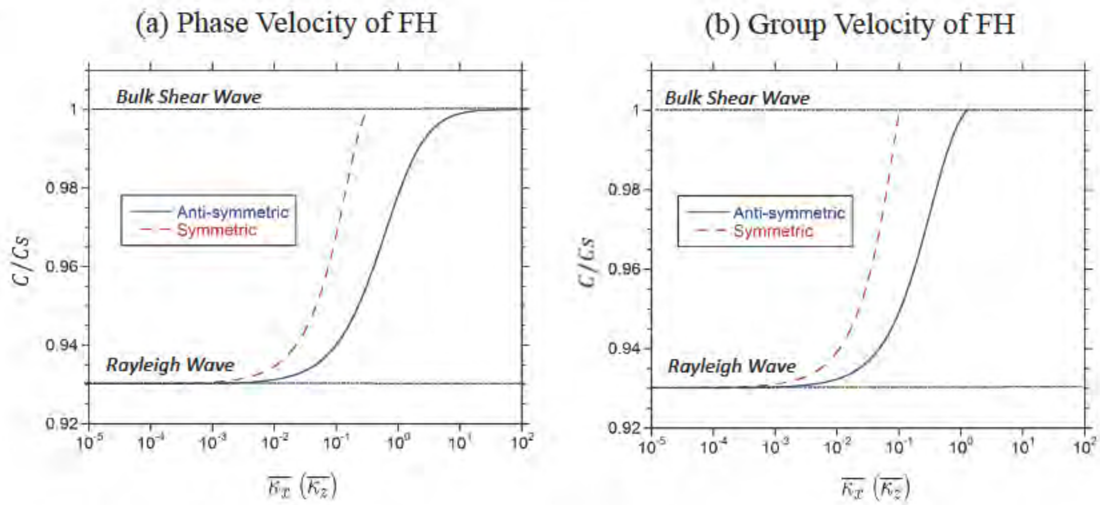

FIG. 4. *(a) Normalized interface wave phase velocity (C/C_S) as a function of normalized stiffness $\overline{\kappa_z} = \kappa_z/\omega Z_S$ for the FH medium; (b) Normalized interface wave group velocity as a function of normalized stiffness $\overline{\kappa_z}$.*

waves polarized perpendicular to layers (referred to as the SV wave with a velocity of v_{SV}):

$$C_{66} = \rho v_{SH}^2, \quad C_{44} = \rho v_{SV}^2, \tag{3.2}$$

where γ can be rewritten as:

$$\gamma = \frac{1}{2}\left[\left(\frac{v_{SH}}{v_{SV}}\right)^2 - 1\right], \tag{3.3}$$

Figure 5a shows the theoretical ratio of v_{SH} to v_{SV} (indicator of shear wave anisotropy exhibiting similar trends to γ) as a function of fracture specific stiffness. When interface waves are present, the matrix anisotropy is masked at low values of fracture specific stiffness. As stress on a fracture is increased, fracture specific stiffness increases because of the increase in contact area between the two surfaces and the reduction in aperture. For the FH medium, the ratio v_{SH}/v_{SV} increases from nearly isotropic ($v_{SH}/v_{SV} \sim 1$) to the background anisotropy ($v_{SH}/v_{SV} \sim 1.06$) with increasing stiffness. Conversely, when the fracture is perpendicular to the layers (the FV medium), the apparent anisotropy decreases from 1.12 to 1.06, i.e. to the ratio of v_{SH} to v_{SV} of the layered matrix. This demonstrates theoretically that the presence of fractures in a layered medium can lead to the misinterpretation of the shear wave anisotropy when fracture interface waves are present, but not recognized.

Previous experimental results (Figure 5b) also showed that the interpretation of shear-wave splitting or shear-wave anisotropy for a fractured layered medium depends on the orientation of the fracture (Shao et al., 2012): the ratio of the SH wave velocity to the SV wave velocity is approximately 1.06 and is independent of stress, for an intact sample or the intact portion of both the fractured samples, when waves propagated parallel to the layering. However, if a fracture is oriented perpendicular to the layering, the layered medium appears almost isotropic at low stress but recovers the matrix anisotropy at high stress (blue circles in Figure 5b). Conversely, if a fracture is oriented parallel to the layering, the layered medium appears more anisotropic at low stress and also recovers the matrix anisotropy at high stress (black squares in Figure 5b).

Theoretical results exhibits close values and trends as the experimental ones. Thus the existence of fracture interface waves can mask the matrix anisotropy of a medium if the fractures are not sufficiently closed and if those guided modes are not identified.

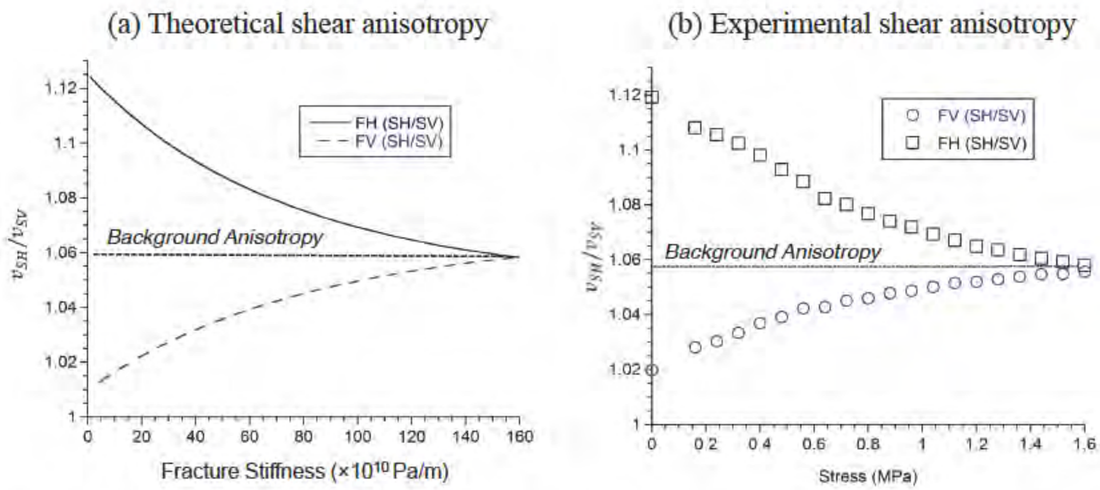

FIG. 5. *(a) Theoretical shear anisotropy of the FH and FV media as a function of fracture specific stiffness; (b) Experimental shear stiffness as a function of external normal stress.*

3.2. Shear specific stiffness estimation. As mentioned, fracture interface waves are a form of generalized coupled Rayleigh waves that travel with a velocity that ranges between the Rayleigh wave velocity and the bulk shear wave velocity. The velocity of a fracture interface wave is controlled by the properties of the matrix (density, seismic impedance) and the specific stiffness of the fracture. Fracture specific stiffness depends directly on the amount and distribution of contact area between the two fracture surfaces and is affected by the aperture distribution (Pyrak-Nolte et al., 2000). There are two types of non-evanescent interface waves: symmetric (fast wave) and antisymmetric (slow wave) waves (Pyrak-Nolte, 1987; Gu, 1994; Nihei, 1994). In this study, we observed the antisymmetric or slow interface that only depends on the shear stiffness of the fracture. Our assumption that we are only observing the antisymmetric mode is based on the simulation work of Nihei et al. (see Nihei et al., 1994) that showed that the antisymmetric mode is best generated by a vertically polarized source (vertical to the fracture) such as that used in previous experiments (Shao et al., 2012).

Using the theory for fracture interface waves and the properties of an intact garolite sample, a theoretical curve (Figure 6a) of normalized interface wave velocity, (the interface wave group velocity v_{IW} is normalized by the bulk shear wave velocity v_S), is shown as a function of normalized stiffness, where the stiffness is normalized by the ratio of fracture specific stiffness, κ, to seismic impedance, Z, (phase velocity $\times$density) as in the theoretical section. The curve was generated for a frequency of 0.21 MHz, the frequency at which the group velocities were determined at the largest energy concentration. The value of v_S and Z depend on the polarization of the shear wave source relative to the layering.

Interface waves were observed for the SH waves in the FV medium and the SV waves for the FH medium, that exhibited group velocities in the range of the theoretical fracture interface wave velocities (Figure 6a). From those results, the fracture specific stiffness was estimated and is shown as a function of stress in Figure 6b. For normal stresses less than 1 MPa, the estimated fracture stiffness of the fracture in FV is larger than FH. The difference in fracture specific stiffness at lower stress for the two fractures is attributed to difference in the asperity height distributions. The difference in asperity height occurs because the fracture in sample FV cuts across the layering (i.e. cloth), while the fracture in sample FH is parallel to the layering. The faster increase in stiffness for the FH than the FV fracture indicates that the larger apertures in the fracture are closing. For normal stresses higher than 1.2 MPa, the estimated fracture stiffness is close in value for FV and

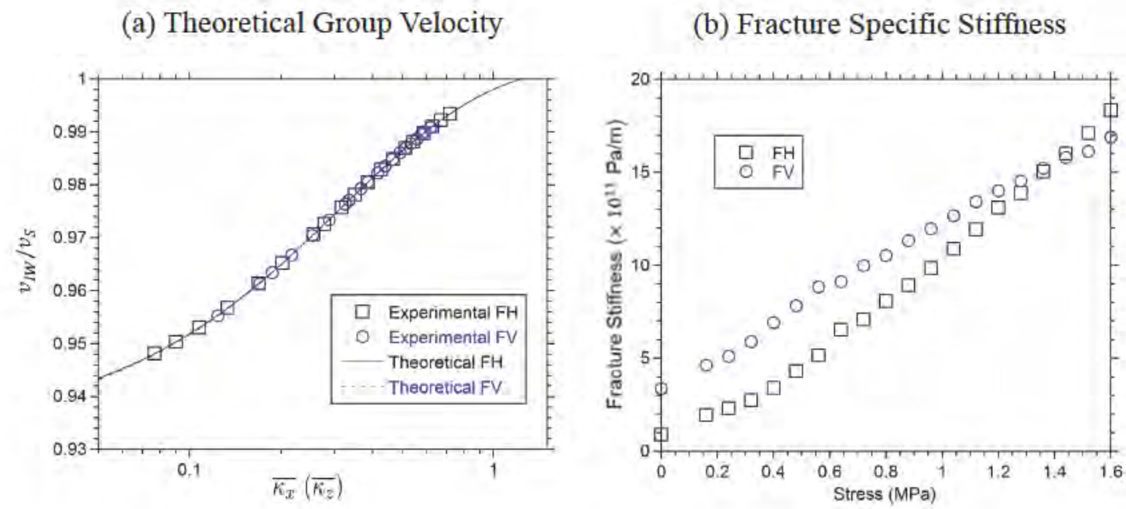

FIG. 6. *(a) Comparison of theoretical normalized group velocity as a function of normalized stiffness for fracture interface waves and measured values. (b) Estimated shear fracture specific stiffness for the fractures in the FV and FH media.*

FH, which indicates a sufficient closing of the fractures. The interpreted fracture shear stiffness is consistent with the geometrical properties of the surfaces.

4. Conclusions. The question arises whether competing sources of anisotropy can be delineated for an anisotropic medium containing fractures. The results reported here demonstrate that the presence of a fracture can mask the matrix anisotropy caused by layering, because of discrete guided-modes that occur along fractures. A medium can appear more or less anisotropic depending on the orientation of the fracture relative to the layering. More importantly, the matrix anisotropy can be recovered by increasing the fracture specific stiffness through the application of stress, i.e. closing the fracture. Ignoring the presence of guided-modes in the fractured medium can result in errors in interpretation of fracture orientation and matrix anisotropy.

Acknowledgements. The authors wish to acknowledge support of this work by the Geosciences Research Program, Office of Basic Energy Sciences US Department of Energy (DE-FG02-09ER16022), and the Geo-mathematical Imaging group at Purdue University.

Appendix 5. Derivation of interface waves for the FV medium. The FV Medium has a fracture lying in the x-y plane, and its symmetric axis of the layering is along the y axis (Figure 1). Waves propagate along the x axis without y components, but with exponentially decaying amplitude along z direction. The geometry of this problem can be simplified only in the x-z plane as Figure A1, and the potential for the fracture interface wave can be expressed as:

$$\begin{aligned} \phi^{(1)} &= A^{(1)} \exp\left[-p\omega z + \mathrm{i}\omega(x/C - t)\right],\ z \geq 0 \\ \phi^{(2)} &= A^{(2)} \exp\left[p\omega z + \mathrm{i}\omega(x/C - t)\right],\ z \leq 0 \end{aligned} \tag{5.1}$$

for the P wave, and

$$\begin{aligned} \psi^{(1)} &= B^{(1)} \exp\left[-q\omega z + \mathrm{i}\omega(x/C - t)\right],\ z \geq 0 \\ \psi^{(2)} &= B^{(2)} \exp\left[q\omega z + \mathrm{i}\omega(x/C - t)\right],\ z \leq 0 \end{aligned} \tag{5.2}$$

for the sS wave, where superscripts (1) and (2) refer to media 1 and 2, ω is the angular frequency,t is time, $A^{(1)}, A^{(2)}, B^{(1)}$ and $B^{(2)}$ are constants that need to be determined, C is the interface wave velocity we are looking for, p and q are expressed as:

$$p = \sqrt{\frac{1}{C^2} - \frac{1}{C_P^2}},$$
$$q = \sqrt{\frac{1}{C^2} - \frac{1}{C_S^2}}, \tag{5.3}$$

where C_P and C_S are P and S wave velocities.

The particle displacement can be obtained by:

$$\begin{aligned} u_x^{(1)} &= \frac{\partial \phi^{(1)}}{\partial x} - \frac{\partial \psi^{(1)}}{\partial z}, \\ u_z^{(1)} &= \frac{\partial \phi^{(1)}}{\partial z} + \frac{\partial \psi^{(1)}}{\partial x}, \\ u_x^{(2)} &= \frac{\partial \phi^{(2)}}{\partial x} - \frac{\partial \psi^{(2)}}{\partial z}, \\ u_z^{(2)} &= \frac{\partial \phi^{(2)}}{\partial z} + \frac{\partial \psi^{(2)}}{\partial x}. \end{aligned} \tag{5.4}$$

Hook's law is used to relate stress ($\boldsymbol{\sigma}$) and strain ($\boldsymbol{\epsilon}$) via elastic stiffness tensor $\boldsymbol{C}$:

$$\boldsymbol{\sigma} = \boldsymbol{C} \cdot \boldsymbol{\epsilon}, \tag{5.5}$$

Voigt's notation $(xx \to 1, yy \to 2, zz \to 3, yz(zy) \to 4, xz(zx) \to 5, xy(yx) \to 6)$ transformed the stress and strain tensor ($\boldsymbol{\sigma}$ and $\boldsymbol{\epsilon}$) into vectors as

$$\begin{aligned} \boldsymbol{\sigma} &= (\sigma_{xx}, \sigma_{yy}, \sigma_{zz}, \sigma_{yz}, \sigma_{zx}, \sigma_{xy})^T = (\sigma_1, \sigma_2, \sigma_3, \sigma_4, \sigma_5, \sigma_6)^T, \\ \boldsymbol{\epsilon} &= (\epsilon_{xx}, \epsilon_{yy}, \epsilon_{zz}, \epsilon_{yz}, \epsilon_{zx}, \epsilon_{xy})^T = (\epsilon_1, \epsilon_2, \epsilon_3, \epsilon_4, \epsilon_5, \epsilon_6)^T, \end{aligned} \tag{5.6}$$

and $\boldsymbol{C}$ into a 6×6 second rank tensor (y-axis symmetry for the matrix):

$$\boldsymbol{C} = \begin{pmatrix} C_{11} & C_{13} & (C_{11} - 2C_{66}) & 0 & 0 & 0 \\ C_{13} & C_{33} & C_{13} & 0 & 0 & 0 \\ (C_{11} - 2C_{66}) & C_{13} & C_{11} & 0 & 0 & 0 \\ 0 & 0 & 0 & C_{44} & 0 & 0 \\ 0 & 0 & 0 & 0 & C_{66} & 0 \\ 0 & 0 & 0 & 0 & 0 & C_{44} \end{pmatrix}. \tag{5.7}$$

Then we express normal and shear stress for Media 1 and 2 in the form of displacement as:

$$\begin{aligned} \sigma_{zz}^{(1)} &= (C_{11} - 2C_{66}) \frac{\partial u_x^{(1)}}{\partial x} + C_{11} \frac{\partial u_z^{(1)}}{\partial z}, \\ \sigma_{xz}^{(1)} &= C_{66} \left(\frac{\partial u_x^{(1)}}{\partial z} + \frac{\partial u_z^{(1)}}{\partial x} \right), \\ \sigma_{zz}^{(2)} &= (C_{11} - 2C_{66}) \frac{\partial u_x^{(2)}}{\partial x} + C_{11} \frac{\partial u_z^{(2)}}{\partial z}, \\ \sigma_{xz}^{(2)} &= C_{66} \left(\frac{\partial u_x^{(2)}}{\partial z} + \frac{\partial u_z^{(2)}}{\partial x} \right), \end{aligned} \tag{5.8}$$

where C_{11} and C_{66} can be expressed by wave velocities C_S, C_P and material density ρ as:

$$\begin{aligned} C_{11} &= \rho C_P^2, \\ C_{66} &= \rho C_S^2. \end{aligned} \tag{5.9}$$

Applying the boundary conditions in equation (1) in the body text, 4 linear equations can be obtained as:

$$
\begin{aligned}
&\frac{\mathrm{i}(\kappa_x + 2\omega p\rho C_S^2)}{C} A^{(1)} - \omega\rho C_S^2\left(\frac{1}{C_S^2} - \frac{2}{C^2}\right) B^{(1)} + q\kappa_x B^{(1)} - \frac{\mathrm{i}\kappa_x}{C} A^{(2)} + q\kappa_x B^{(2)} = 0,\\
&\frac{\mathrm{i}(\kappa_z + 2\omega p\rho C_S^2)}{C} B^{(1)} + \omega\rho C_S^2\left(\frac{1}{C_S^2} - \frac{2}{C^2}\right) A^{(1)} - q\kappa_z A^{(1)} - \frac{\mathrm{i}\kappa_z}{C} B^{(2)} + q\kappa_z A^{(2)} = 0,\\
&\frac{2\mathrm{i}p}{C}(A^{(1)} + A^{(2)}) + \left(\frac{1}{C^2} + q^2\right)(B^{(1)} - B^{(2)}) = 0,\\
&\left(\frac{1}{C_S^2} - \frac{2}{C^2}\right)(A^{(1)} - A^{(2)}) + \frac{2\mathrm{i}q}{C}(B^{(1)} + B^{(2)}) = 0.
\end{aligned}
\tag{5.10}
$$

When $A^{(1)} = A^{(2)}, B^{(1)} = -B^{(2)}$, we can get the equation for symmetric interface wave field:

$$
(1-2\xi^2)^2 - 4\xi^2\sqrt{\xi^2-\eta^2}\sqrt{\xi^2-1} - 2\overline{\kappa_z}\sqrt{\xi^2-\eta^2} = 0, \tag{5.11}
$$

and when $A^{(1)} = A^{(2)}, B^{(1)} = -B^{(2)}$, we can get the equation for antisymmetric wave field:

$$
(1-2\xi^2)^2 - 4\xi^2\sqrt{\xi^2-\eta^2}\sqrt{\xi^2-1} - 2\overline{\kappa_x}\sqrt{\xi^2-1} = 0, \tag{5.12}
$$

where $\xi = C_S/C, \eta = C_S/C_P$, normalized normal stiffness $\overline{\kappa_z} = \kappa_z/\omega Z_S$, and shear stiffness $\overline{\kappa_x} = \kappa_x/\omega Z_S$ ($Z_S = \rho C_S$ is the shear wave impedance). The symmetric and antisymmetric wave fields for interface wave are presented in Figure A2.

Appendix 6. Derivation of interface waves for the FH medium. the FH medium has both the fracture and the layering lying in the x-y plane (Figure 3). The geometry of this problem is in Figure B1. The derivation process is similar to that for the FV medium (same forms of wave potential, displacement expression, and boundary conditions). The main difference is from the elastic stiffness tensor for matrix, which now is z-axis symmetric:

$$
\boldsymbol{C} = \begin{pmatrix}
C_{11} & (C_{11}-2C_{66}) & C_{13} & 0 & 0 & 0\\
(C_{11}-2C_{66}) & C_{11} & C_{13} & 0 & 0 & 0\\
C_{13} & C_{13} & C_{33} & 0 & 0 & 0\\
0 & 0 & 0 & C_{44} & 0 & 0\\
0 & 0 & 0 & 0 & C_{44} & 0\\
0 & 0 & 0 & 0 & 0 & C_{66}
\end{pmatrix}. \tag{6.1}
$$

The normal and shear stresses for Media 1 and 2 in the form of displacement are:

$$
\begin{aligned}
\sigma_{zz}^{(1)} &= C_{13}\frac{\partial u_x^{(1)}}{\partial x} + C_{33}\frac{\partial u_z^{(1)}}{\partial z},\\
\sigma_{xz}^{(1)} &= C_{44}\left(\frac{\partial u_x^{(1)}}{\partial z} + \frac{\partial u_z^{(1)}}{\partial x}\right),\\
\sigma_{zz}^{(2)} &= C_{13}\frac{\partial u_x^{(2)}}{\partial x} + C_{33}\frac{\partial u_z^{(2)}}{\partial z},\\
\sigma_{xz}^{(2)} &= C_{44}\left(\frac{\partial u_x^{(2)}}{\partial z} + \frac{\partial u_z^{(2)}}{\partial x}\right),
\end{aligned}
\tag{6.2}
$$

where C_{33} andC_{44} can be expressed by wave velocities C_S^*, C_P^* (propagated perpendicular through layers) and material density ρ as (see Figure 3):

$$
\begin{aligned}
C_{33} &= \rho {C_P^*}^2,\\
C_{44} &= \rho {C_S^*}^2.
\end{aligned}
\tag{6.3}
$$

The off diagonal component C_{13} are more complicated. It relates to azimuthally-varied wave velocities. For simplicity in this derivation, we express C_{13} in terms of a notation C'_S:

$$C_{13} = C_{33} - 2\rho C'^2_S. \tag{6.4}$$

The method to obtain C_{13} and C'_S will be introduced in body text (in Section 2). Using the boundary condition in equation (1), 4 linear equations are obtained:

$$\begin{aligned}
&\frac{\mathrm{i}(\kappa_x + 2\omega p\rho C^{*\,2}_S)}{C} A^{(1)} - \omega\rho C^{*\,2}_S \left(\frac{1}{C_S^2} - \frac{2}{C^2}\right) B^{(1)} + q\kappa_x B^{(1)} - \frac{\mathrm{i}\kappa_x}{C} A^{(2)} + q\kappa_x B^{(2)} = 0,\\
&\frac{\mathrm{i}(\kappa_z + 2\omega p\rho C'^2_S)}{C} B^{(1)} + \omega\rho \left(\frac{C^{*\,2}_P}{C_P^2} - \frac{2C'^2_S}{C^2}\right) A^{(1)} - q\kappa_z A^{(1)} - \frac{\mathrm{i}\kappa_z}{C} B^{(2)} + q\kappa_z A^{(2)} = 0,\\
&\frac{2\mathrm{i}p}{C}(A^{(1)} + A^{(2)}) + \left(\frac{1}{C^2} + q^2\right)(B^{(1)} - B^{(2)}) = 0,\\
&\left(\frac{C^{*\,2}_P}{C_P^2} - \frac{2C'^2_S}{C^2}\right)(A^{(1)} - A^{(2)}) + \frac{2\mathrm{i}qC'^2_S}{C}(B^{(1)} + B^{(2)}) = 0.
\end{aligned} \tag{6.5}$$

When $A^{(1)} = A^{(2)}, B^{(1)} = -B^{(2)}$, we can get the equation for a symmetric interface wave field as:

$$\left(\frac{\eta_3}{\eta_1}\right)^2 \left[(2\xi^2 - 1)\left(2\xi^2 - \left(\frac{\eta_1\eta_2}{\eta_3}\right)^2\right) - 4\xi^2\sqrt{\xi^2 - 1}\sqrt{\xi^2 - \eta_1^2}\right] - 2\sqrt{\xi^2 - \eta_1^2}\cdot\overline{\kappa_z} = 0, \tag{6.6}$$

When $A^{(1)} = -A^{(2)}, B^{(1)} = B^{(2)}$, we can get the equation for an antisymmetric wave field as:

$$\left(\frac{\eta_3\eta_4}{\eta_1^2\eta_2}\right)^2 \left[(2\xi^2 - 1)\left(2\xi^2 - \left(\frac{\eta_1\eta_2}{\eta_3}\right)^2\right) - 4\xi^2\sqrt{\xi^2 - 1}\sqrt{\xi^2 - \eta_1^2}\right] - 2\sqrt{\xi^2 - 1}\cdot\overline{\kappa_x} = 0, \tag{6.7}$$

where

$$\begin{aligned}
\xi &= C_S/C,\\
\eta_1 &= C_S/C_P,\\
\eta_2 &= C^*_P/C_P,\\
\eta_3 &= C'_S/C_P,\\
\eta_4 &= C^*_S/C_P,
\end{aligned} \tag{6.8}$$

C is the interface wave velocity, and normalized normal stiffness $\overline{\kappa_z} = \kappa_z/\omega Z_S$, and shear stiffness $\overline{\kappa_x} = \kappa_x/\omega Z_S$ ($Z_S = \rho C_S$ is the shear wave impedance).

REFERENCES

[1] J. M. Carcioné, *Elastodynamics of a non-ideal interface: application to crack and fracture scattering*, J. Geophys. Res., 101 (1996), pp. 28177–28188.

[2] ———, *Reflection and transmission of qP-qS plane waves at a plane boundary between viscoelastic transversely isotropic media*, Geophys. J. Int., 129 (1997), pp. 669–680.

[3] ———, *Scattering of elastic waves by a plane crack of finite width in a transversely isotropic medium*, Int. J. Numer. Anal. Methods Geomech., 22 (1998), pp. 263–275.

[4] J. M. Carcioné and S. Picotti, *Reflection and transmission coefficients of a fracture in transversely isotropic media*, Stud.Geophysics. Geod., 56 (2012), pp. 307–322.

[5] S. Chaisri and E. S. Krebes, *Exact and approximate formulas for p-sv reflection and transmission coefficients for a nonwelded contact interface*, J. Geophys. Res., 105 (2000), pp. 28045–28054.

[6] C. Diner, *Decomposition of compliance tensor for fractures and transversely isotropic medium.* In Proceedings of the journal Geophysical Prospecting, Nov. 2011.

[7] B. Gu, *Interface waves on a fracture in rock*, PhD thesis, University of California, Berkeley, 1994.

[8] B. Gu, K. T. Nihei, L. R. Myer, and L. J. Pyrak-Nolte, *Fracture interface waves*, J. Geophys. Res., 101 (1996), pp. 827–835.
[9] K. Kendall and D. Tabor, *An ultrasonic study of the area of contact between stationary and sliding surfaces*, Uproc. Royal Soc. London, Series A, 323 (1971), pp. 321–340.
[10] C. Kitsunezaki, *Behavior of plane waves across a plane crack*, J. Mining Coll. Akita Univ, series A, 3 (1983), pp. 173–187.
[11] T. Kundu and A. Boström, *Elastic wave scattering by a circular crack in a transversely isotropic solid*, Wave Motion, 15 (1992), pp. 285–300.
[12] R. D. Mindlin, *Waves and vibrations in isotropic planes*, J.W. Goodier and W.J. Hoff, Editors, 1960.
[13] G. S. Murty, *A theoretical model for the attenuation and dispersion of stoneley waves at the loosely bonded interface of elastic half-spaces*, Phys. Earth Planet. In., 11 (1975), pp. 65–79.
[14] G. S. Murty and V. Kumar, *Elastic wave propagation with kinematic discontinuity along a non-ideal interface between two isotropic elastic half-spaces*, Journal of Nondestructive Evaluation, 11 (1991), pp. 39–53.
[15] L. R. Myer, D. L. Hopkins, and N. G. W. Cook, *Effects of contact area of an interface on acoustic wave transmission characteristics*, in the US Rock Mechanics Symposium, 1985.
[16] K. T. Nihei, L. R. Myer, N. G. W. Cook, and W. D. Yi, *Effects of nonwelded interfaces on guided sh-waves*, Geophys. Res. Lett., 21 (1994), pp. 745–748.
[17] K. T. Nihei, W. Yi, L. R. Myer, and N. G. W. Cook, *Fracture channel waves*, J. Geophys. Res., 10 (1999), pp. 4749–4781.
[18] D. D. Nolte, L. J. Pyrak-Nolte, J. Beachy, and C. Ziegler, *Transition from the displacement discontinuity limit to resonant scattering regime for fracture interface waves*, Int. J. Rock Mech. Min. Sci., 37 (2000), pp. 219–230.
[19] L. J. Pyrak-Nolte, *Seismic visibility of fractures*, PhD thesis, University of California, Berkeley, 1988.
[20] L. J. Pyrak-Nolte and J. P. Morris, *Single fractures under normal stress: the relation between fracture specific stiffness and fluid flow*, Int. J. Rock Mech. Min. Sci., 37 (2000), pp. 245–262.
[21] L. J. Pyrak-Nolte, L. R. Myer, and N. G. W. Cook, *Transmission of seismic-waves across single natural fractures*, J. GEOPHYS. RES.-SOLID, 95 (1990), pp. 8617–8638.
[22] L. J. Pyrak-Nolte and D. D. Nolte, *Wavelet analysis of velocity dispersion of elastic interface waves propagating along a fracture*, Geophys. Res. lett., 22 (1995), pp. 1329–1332.
[23] A. Rüger, *Variation of P-wave reflectivity with offset and azimuth in anisotropic media*, Geophysics, 63 (1998), pp. 935–947.
[24] M. Schoenberg, *Elastic wave behavior across linear slip interfaces*, J. Acoust. Soc. Am., 68 (1980), pp. 1516–1520.
[25] ———, *Reflection of elastic waves from periodically stratified media with interfacial slip*, Geophysics, 31 (1983), pp. 265–292.
[26] ———, *Vertically fractured transversely isotropic media: dimensionality and deconstruction*, GEOPHYS. PROSPECT., 57 (2009), pp. 169–185.
[27] S. Shao, B. C. Abell, and L. J. Pyrak-Nolte, *Interface waves along fractures in anisotropic media.* In Proceedings of project review, Geo-Mathematical Imaging Group, 2012.
[28] R. Suarez-Rivera, *The influence of thin clay layers containing liquids on the propagation of shear waves*, PhD thesis, University of California, Berkeley, 1992.
[29] L. Thomsen, *Weak elastic anisotropy*, GEOPHYSICS, 51 (2009), pp. 1954–1966.
[30] C. Xian, D. D. Nolte, and L. J. Pyrak-Nolte, *Compressional waves guided between parallel fractures*, Int. J. Rock Mech. Min. Sci., 38 (2001), pp. 765–776.